

Cell Chemical Biology

Diverse Chemical Scaffolds Enhance Oligodendrocyte Formation by Inhibiting CYP51, TM7SF2, or EBP

Highlights

- A small-molecule screen identified novel enhancers of oligodendrocyte formation
- Most top compounds target cholesterol biosynthesis enzymes CYP51, TM7SF2, or EBP
- Evaluation of analogs identified CW3388 as a potent, selective EBP inhibitor
- CW3388 is poised for further optimization toward EBP-targeting remyelinating drugs

Authors

Dharmaraja Allimuthu, Zita Hubler, Fadi J. Najm, ..., William Seibel, Paul J. Tesar, Drew J. Adams

Correspondence

drew.adams@case.edu

In Brief

Demyelinating diseases are characterized by oligodendrocyte loss. A small-molecule screen uncovered novel enhancers of oligodendrocyte formation. Most hits inhibit a narrow range of enzymes in the cholesterol biosynthesis pathway. Structure-activity relationship studies identified CW3388, a potent EBP inhibitor poised for optimization as a remyelinating therapeutic.

Diverse Chemical Scaffolds Enhance Oligodendrocyte Formation by Inhibiting CYP51, TM7SF2, or EBP

Dharmaraja Allimuthu,^{1,5} Zita Hubler,^{1,5} Fadi J. Najm,¹ Hong Tang,² Ilya Bederman,³ William Seibel,⁴ Paul J. Tesar,¹ and Drew J. Adams^{1,6,*}

¹Department of Genetics and Genome Sciences, Case Western Reserve University School of Medicine, Cleveland, OH 44106, USA

²Drug Discovery Center, University of Cincinnati College of Medicine, Cincinnati, OH 45237, USA

³Department of Pediatrics, Case Western Reserve University School of Medicine, Cleveland, OH 44106, USA

⁴Oncology Department, Cincinnati Children's Hospital Medical Center, Cincinnati, OH 45229, USA

⁵These authors contributed equally

⁶Lead Contact

*Correspondence: drew.adams@case.edu

<https://doi.org/10.1016/j.chembiol.2019.01.004>

SUMMARY

Small molecules that promote oligodendrocyte formation have been identified in “drug repurposing” screens to nominate candidate therapeutics for diseases in which myelin is lost, including multiple sclerosis. We recently reported that many such molecules enhance oligodendrocyte formation not by their canonical targets but by inhibiting a narrow range of enzymes in cholesterol biosynthesis. Here we identify enhancers of oligodendrocyte formation obtained by screening a structurally diverse library of 10,000 small molecules. Identification of the cellular targets of these validated hits revealed a majority inhibited the cholesterol biosynthesis enzymes CYP51, TM7SF2, or EBP. In addition, evaluation of analogs led to identification of CW3388, a potent EBP-inhibiting enhancer of oligodendrocyte formation poised for further optimization.

INTRODUCTION

Myelin is a lipid-rich membrane produced by oligodendrocytes that wraps around central nervous system (CNS) axons (Bechler et al., 2015). Multiple CNS diseases including multiple sclerosis (MS) are characterized by the loss of myelin and oligodendrocytes (Lassmann, 2001; Fancy et al., 2010). Myelin loss can in some contexts be repaired via the differentiation of oligodendrocyte progenitor cells (OPCs) to new oligodendrocytes (Keirstead and Blakemore, 1999; Franklin and Ffrench-Constant, 2008). However, endogenous “remyelination” is often insufficient to halt disease progression.

Multiple studies have used high-throughput chemical screening of bioactive libraries as a “drug repurposing” approach to identify small molecules that enhance oligodendrocyte formation *in vitro* and promote functional remyelination in animal models of MS (Hubler et al., 2018; Najm et al., 2015; Deshmukh et al., 2013; Mei et al., 2014, 2016; Huang et al.,

2011; Gonzalez et al., 2016; Lariosa-Willingham et al., 2016). Recently, we established that more than two dozen of these screening hits enhance oligodendrocyte formation by inhibiting a narrow range of steps in cholesterol biosynthesis—sterol-C14-demethylase (CYP51), sterol-14-reductase (TM7SF2), and Δ 8,7-sterol isomerase (EBP)—and inducing accumulation of 8,9-unsaturated sterols (Hubler et al., 2018).

We have now screened 10,000 chemically diverse small molecules for enhancers of oligodendrocyte formation. In line with past repurposing screens, we find that a majority of validated hits inhibit either CYP51, TM7SF2, or EBP. Evaluation of a large collection of analogs of one series of hits confirmed that potency for inhibition of EBP correlated closely with potency for enhanced oligodendrocyte formation. In addition, we identified CW3388, a substantially more potent EBP inhibitor.

RESULTS

We screened our established high-content imaging assay measuring the differentiation of OPCs to myelin basic protein-positive (MBP+) oligodendrocytes (Najm et al., 2015) against a library of 10,000 structurally diverse small molecules at a uniform dose of 10 μ M (Figures 1A and 1B). From this library, 78 potential hit molecules were selected for further evaluation on the basis of enhanced formation of MBP+ oligodendrocytes (see the STAR Methods for detailed hit-calling criteria; hits highlighted in green, Figure 1B). These 78 putative hit molecules were then re-evaluated in two independent derivations of mouse epiblast stem cell-derived OPCs and also assayed for chemical purity, ultimately leading to a set of nine validated hits prioritized for further study (Figures 1C, 1D, and S1A).

As our recent work established inhibition of specific cholesterol pathway enzymes as the functional mechanism by which many small molecules enhance oligodendrocyte formation (Hubler et al., 2018), we next characterized the ability of our screening hits to inhibit cholesterol biosynthesis in OPCs at the screening dose (for a detailed cholesterol biosynthesis pathway map, see Data S1). We used gas chromatography/mass spectrometry (GC-MS) to quantitate levels of cholesterol and 14 cholesterol pathway intermediates in OPCs (Korade et al.,

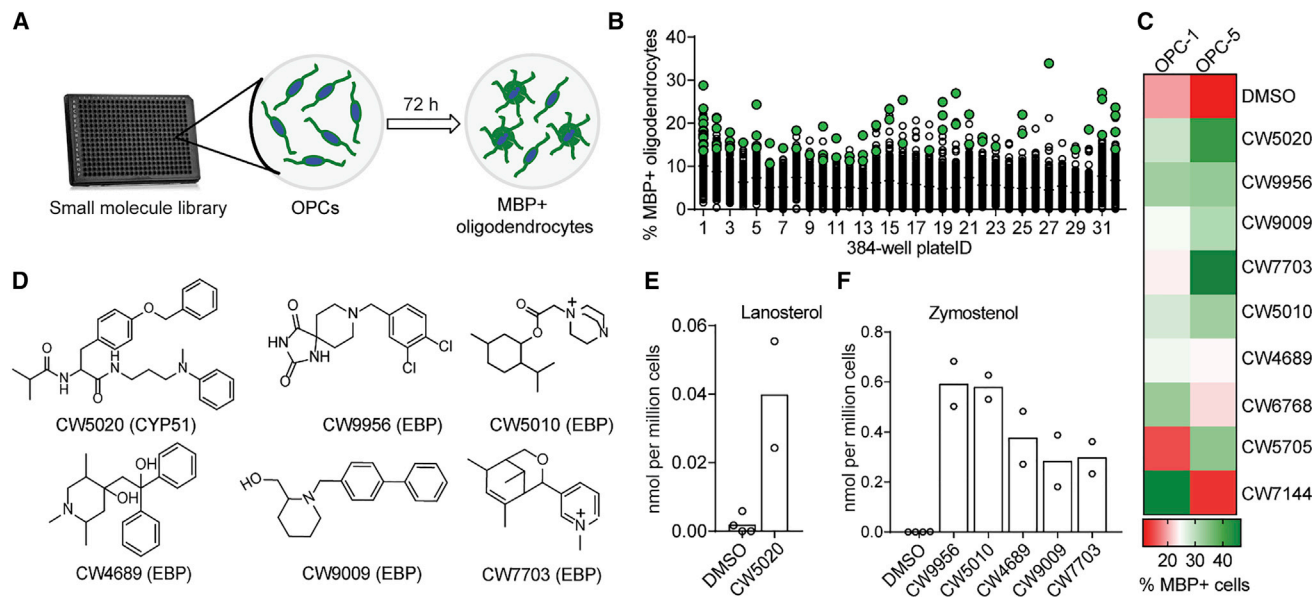


Figure 1. Most Validated Hits Inhibit CYP51 or EBP and Accumulate 8,9-Unsaturated Sterols in OPCs

(A) Schematic representation of screening strategy.

(B) Dot-scattered plot of percentage of MBP+ oligodendrocytes generated after 72 h of treatment. Retested molecules are green.

(C) Heatmap representing percentage of MBP+ oligodendrocytes generated in two derivations of OPCs after treatment with top hits.

(D) Structure of CYP51 or EBP inhibitors identified. See Figure S1 for remaining hits.

(E and F) GC-MS-based quantification of lanosterol (E) and zymostenol (F) after treatment with indicated molecules.

In experiments (C, E, and F), $n = 2$ replicates per condition. All treatments 10 μ M. See also Figure S1.

2016; Giera et al., 2015). Interestingly, GC-MS analysis identified six out of nine molecules as causing inhibition of cholesterol biosynthesis (Figures 1D–1F and S1B). One molecule led to accumulation of the 8,9-unsaturated sterol lanosterol, indicative of CYP51 inhibition (Figures 1D and 1E). Accumulation of zymostenol was observed for five molecules, indicating EBP inhibition (Figures 1D and 1F). These studies further establish that a large fraction of high-throughput screening hits that promote oligodendrocyte formation inhibit CYP51 or EBP.

Next we evaluated all nine validated hits across a wide concentration range to determine their potency for enhancing oligodendrocyte formation (Figure S1C). These studies revealed CW5020, CW9956, and CW9009 as maximally potent promoters of oligodendrocyte formation, with half maximal effective concentration values in the mid-nanomolar range (Figures 2B–2D). CW5020 was initially characterized as inhibiting CYP51 in OPCs, while CW9956 and CW9009 targeted EBP (Figures 1D–1F). As inhibition of cytochrome P450 enzymes often presents challenges for drug discovery efforts, we chose to characterize CW9956 and CW9009. GC-MS analysis across a wider range of concentrations revealed that the potency for EBP inhibition—indicated by accumulation of zymostenol as well as reductions in the basal sterols cholesterol and desmosterol—closely mirrored the potency for oligodendrocyte formation for these molecules (Figures 2C–2F and S2). CW9956 also inhibited EBP in an established enzymatic assay, confirming direct targeting of EBP (Figure 2G) (Moebius et al., 1998).

Mechanistically, we previously established that oligodendrocyte formation is promoted by accumulation of 8,9-unsaturated sterols, whether induced by small-molecule inhibition of CYP51,

TM7SF2, or EBP, or by supplying purified 8,9-unsaturated sterols directly to OPCs (Hubler et al., 2018). Two additional experiments support that accumulation of 8,9-unsaturated sterols resulting from EBP inhibition is also essential for the efficacy of CW9956 in OPCs. First, we previously showed that the accumulation of 8,9-unsaturated sterols can be prevented by complete inhibition of cholesterol biosynthesis at lanosterol synthase using Ro 48-8071 (Figure 2A) (Hubler et al., 2018). Co-treating CW9956 with Ro 48-8071 effectively blocked CW9956's ability to promote oligodendrocyte formation (Figures 2A and 2H). Second, co-treatment of the CYP51 inhibitor ketoconazole with CW9956 did not further enhance oligodendrocyte formation compared with ketoconazole alone (Figure 2H). Since ketoconazole inhibits cholesterol biosynthesis upstream of EBP and leads to accumulation of the 8,9-unsaturated sterol lanosterol, this finding suggests that accumulation of 8,9-unsaturated sterols is a redundant mechanism for these molecules. These experiments indicate that CW9956 enhances oligodendrocyte formation through inhibition of EBP and accumulation of EBP's 8,9-unsaturated sterol substrate zymostenol.

The presence of a common N-benzylpiperidine scaffold in both CW9956 and CW9009 led us to evaluate a focused library of 76 structural analogs of these lead molecules across a wide concentration range. This structure-activity relationship analysis identified analogs whose ability to enhance oligodendrocyte formation was improved or diminished relative to the lead molecules (Figure 3A; Data S2). First, analysis of analogs of CW9009 revealed the azacyclooctane-containing derivative CW3388 showed optimal efficacy for enhancing oligodendrocyte formation among all analogs tested, with

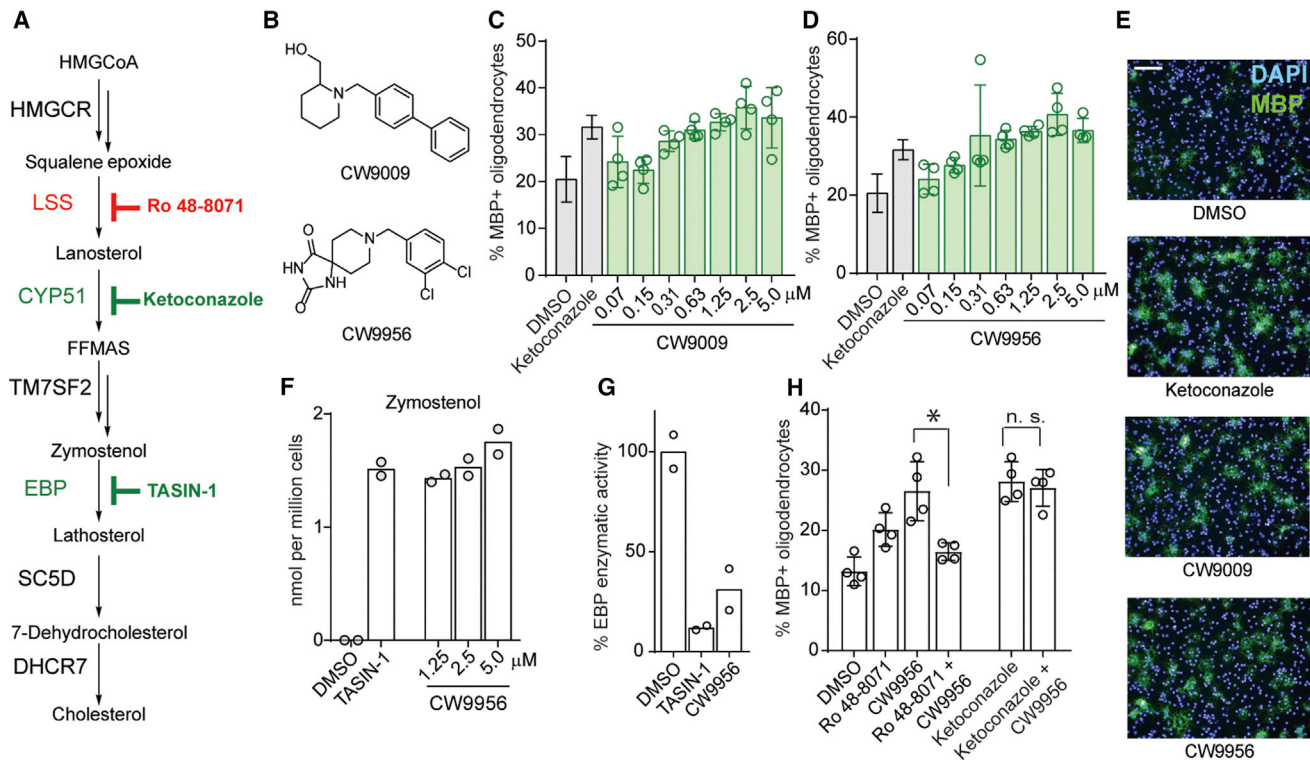


Figure 2. CW9956 and CW9009 Enhance Oligodendrocyte Formation by Inhibiting EBP and Causing Zymostenol Accumulation

(A) Cholesterol biosynthesis pathway in brief.

(B) Structure of CW9009 and CW9956.

(C and D) Percentage of MBP+ oligodendrocytes generated following treatment with CW9009 and CW9956.

(E) Representative images following treatments at 5 μM. Scale bar, 100 μm.

(F) Zymostenol levels in OPC-5 after treatment with CW9956.

(G) EBP enzymatic activity in a biochemical assay; treatments, 10 μM.

(H) Percentage of MBP+ oligodendrocytes following treatment with the indicated small molecules or combinations of small molecules (Ro 48-8071, 11 nM, ketoconazole 2.5 μM, CW9956, 1 μM). $P = 0.0076$ for a combination of Ro 48-8071 and CW9956 in comparison with CW9956; $P = 0.6509$ for the combination of ketoconazole and CW9956 in comparison with ketoconazole; n.s., not significant, two-tailed Student's *t* test.

Experiments in (C–G) are representative of at least two independent experiments. In (C), (D), and (H): $n = 4$ wells per condition except DMSO and ketoconazole $n = 16$ in (C and D). $n = 2$ replicates per condition in (F and G). Throughout, OPC-5 derivation used unless noted. Data in (C, D, and H) are presented as means \pm SD. See also Figure S2 and Data S1.

near-maximal effects observed at 110 nM, the lowest dose tested (Figures 3B and 3C). Most leading analogs shared the biaryl functionality of CW3388, while analogs with smaller ring substituents or a naphthyl moiety (CW8284) were generally inactive (Figures 3B, 3D, and S3A–S3D). One exception to this trend was CW1143, which, unlike its isomer CW8438, strongly promoted oligodendrocyte formation (Figures 3E, 3F, and 3K). Evaluation of analogs of CW9956 revealed that the piperidine-4-spiro-5'-hydantoin functionality is critical for activity, but did not identify analogs with substantially improved potency (Figures S3E–S3H). In summary, evaluation of the effects of analogs of CW9956 and CW9009 on oligodendrocyte formation has established clear structure-activity relationships and identified several analogs with enhanced or diminished potency.

Next, selected analogs were evaluated for their effects on cholesterol biosynthesis using GC-MS-based sterol profiling in OPCs. First, the eight analogs that most potently enhanced oligodendrocyte formation were assayed at a uniform concentration of 1 μM. All eight analogs were found to inhibit cholesterol

biosynthesis and accumulate 8,9-unsaturated sterols. Seven of the eight small molecules were found to accumulate zymostenol, indicative of EBP inhibition, as previously observed for CW9956 and CW9009 (Figures 3G, 3I, S4A, and S4B). OPCs treated with CW4644 instead accumulated 14-dehydrozymostenol, indicative of inhibition of the upstream enzyme TM7SF2 (Figure 3H).

Next, we selected eight analogs confirmed to not promote oligodendrocyte formation for GC-MS-based sterol profiling. Six of these analogs did not show any effect on cholesterol biosynthesis in OPCs, paralleling their inability to promote oligodendrocyte formation (Figure S4E). Notably, this finding also provides a rationale for the surprising finding that CW1143, but not its close isomer CW8438, enhances oligodendrocyte formation: CW1143, but not CW8438, inhibits EBP in OPCs (Figure 3I). In addition, CW1143 inhibited EBP enzymatic activity *in vitro* (Figure S4D). The remaining two molecules showed accumulation of 7-dehydrocholesterol, indicative of inhibition of 7-dehydrocholesterol reductase (DHCR7), inhibition of which we previously demonstrated does not promote oligodendrocyte

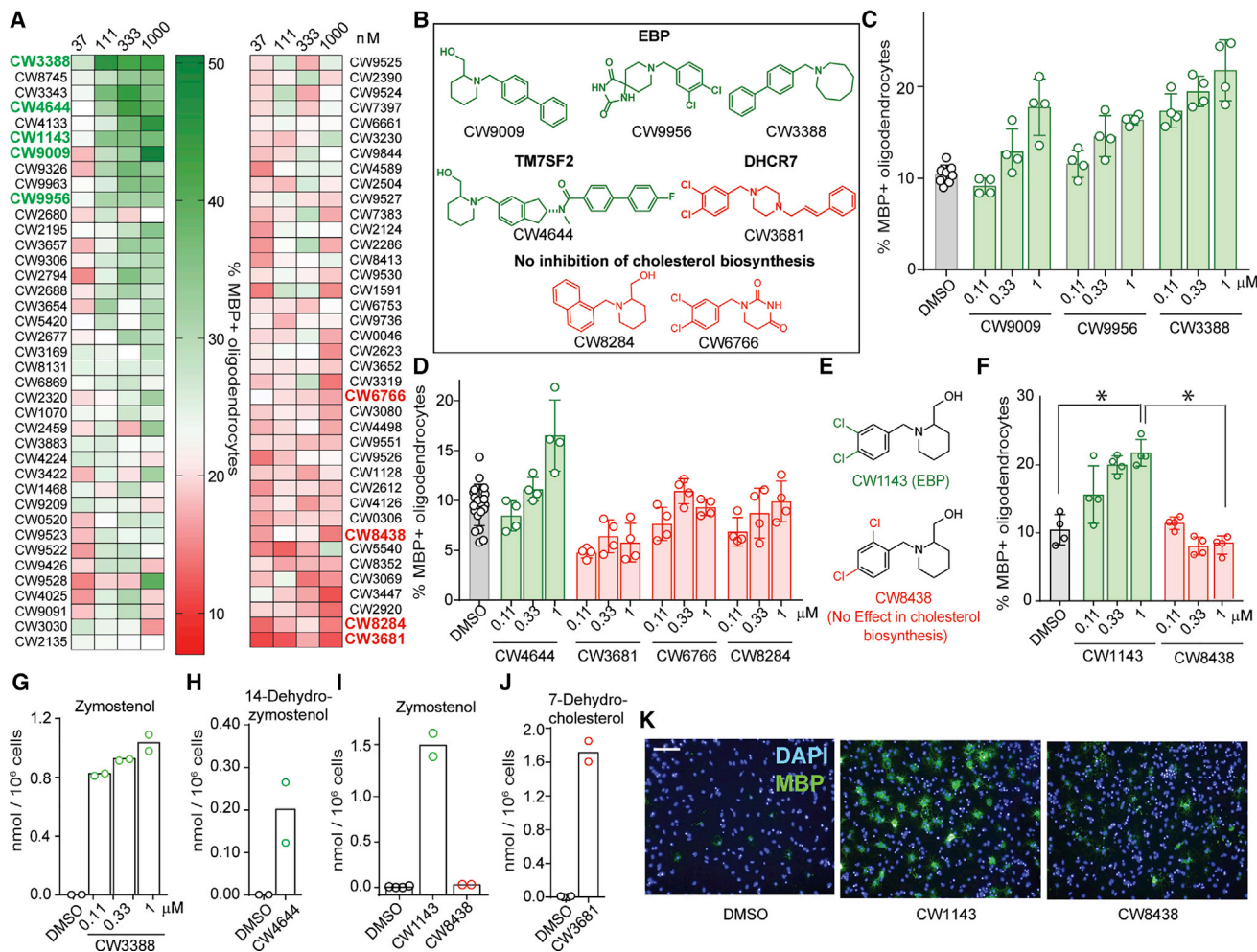


Figure 3. Evaluation of Structural Analogs of CW9956 and CW9009

(A) Heatmap representing percentage of MBP+ oligodendrocytes following treatment with 76 structural analogs of CW9009/CW9956. Structures of molecules labeled in bold are given in (B or E); for all analogs, see [Data S1](#).

(B and E) Molecules discussed in this figure.

(C and D) Percentage of MBP+ oligodendrocytes generated following treatment with the indicated molecules. $n = 4$ wells per condition except DMSO, $n = 8$.

(F) Percentage of MBP+ oligodendrocytes generated following treatment with CW1143 in comparison with CW8438; two-tailed Student's t test, 95% confidence interval. $P = 0.0003$ for CW1143 in comparison with DMSO; $P \leq 0.0005$ for CW1143 in comparison with CW8438.

(G–J) Quantification of zymostenol (G and I), 14-dehydrozymostenol (H), and 7-dehydrocholesterol (J) after treatment with the indicated analogs. $n = 2$ replicates per condition. Each analog was tested at $1 \mu\text{M}$ in (H–J).

(K) Representative images following CW1143 or CW8438 treatment ($1 \mu\text{M}$). Scale bar, $100 \mu\text{m}$.

Data in experiments (C–K) are representative of two or more independent experiments. Data in (C, D, and F) are represented as means \pm SD. See also [Figures S3 and S4](#) and [Data S2](#) and [S3](#). Throughout, green labels indicate enhancers of oligodendrocyte formation; red labels indicate molecules with no effect.

formation ([Figures 3J and S4F](#)). Taken together, this evaluation of 78 structural analogs of CW9009/CW9956 identified several potent enhancers of oligodendrocyte formation that inhibit EBP or TM7SF2.

We further characterized the most potent analog tested, CW3388, which retained near-maximal effects on oligodendrocyte formation at 110 nM , the lowest dose tested ([Figures 3B and 3C](#)). Sterol profiling of OPCs treated with a range of doses of CW3388 confirmed that the enhanced potency for oligodendrocyte formation was matched by improved potency for EBP inhibition in OPCs ([Figure 3G](#)) and in an enzymatic assay ([Figure 4A](#)). In addition, we assessed whether CW3388 could also promote

in vitro “myelination” of an axon-like electrospun microfiber substrate. CW3388 treatment substantially increased the area of microfibers tracked by MBP+ oligodendrocytes, indicating that CW3388 treatment promotes both MBP+ oligodendrocyte formation and subsequent myelination *in vitro* ([Figures 4B–4D](#)). These data support CW3388 as a highly potent, cell-active enhancer of oligodendrocyte formation that functions by EBP inhibition.

Finally, small molecules identified in past screens that function in OPCs by inhibition of EBP, including clemastine, tamoxifen, and U50488, have liabilities associated with modulation of these molecules’ canonical targets that may limit their drug

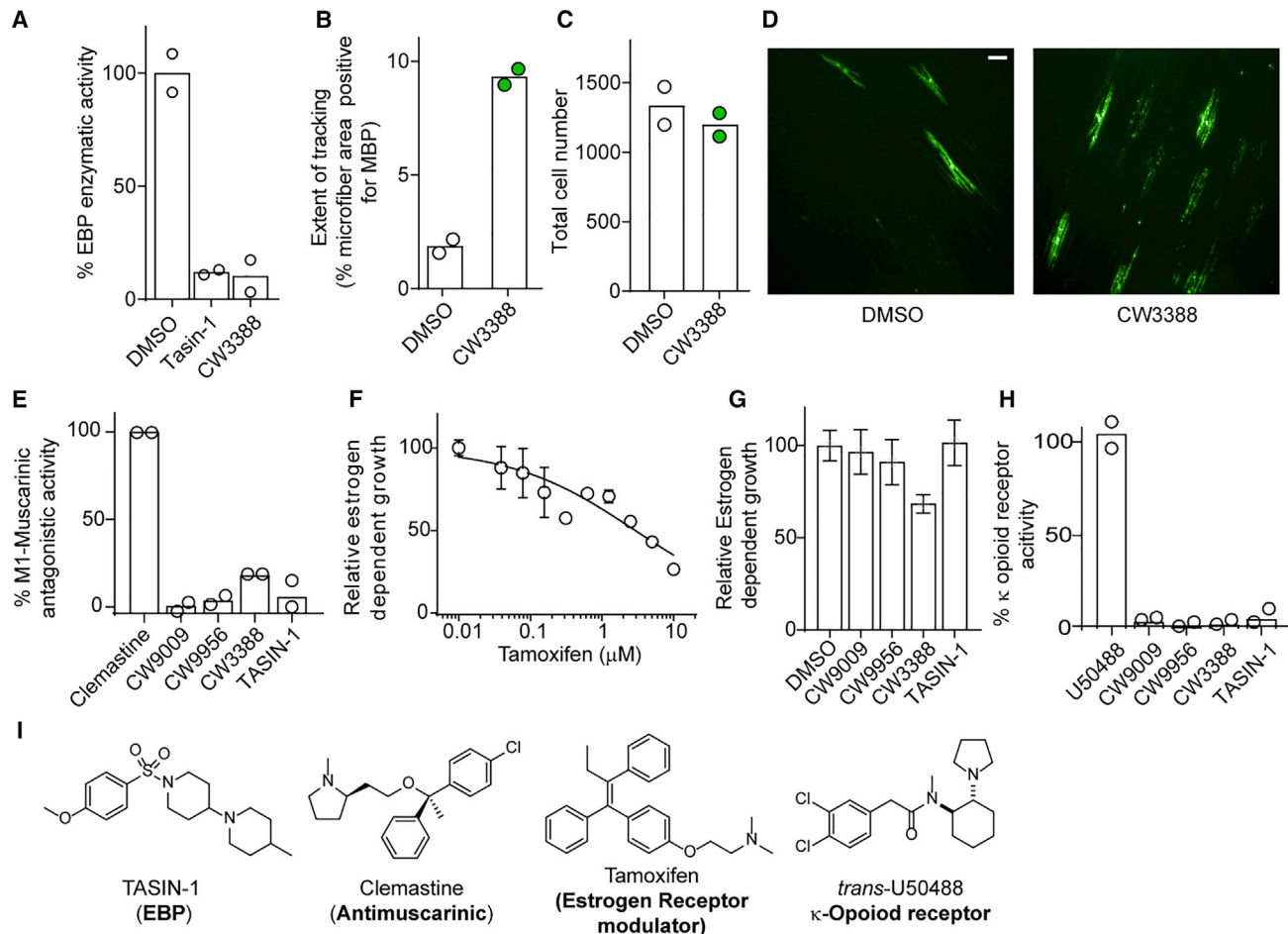


Figure 4. EBP Inhibitors Promote Wrapping of Microfibers but Lack the Potent Off-Target Effects of Molecules Identified in Repurposing Screens

(A) EBP enzymatic activity in a biochemical assay at 10 μ M. n = 2 replicates per condition, representative of two independent experiments.
 (B) Quantification of the area of electrospun microfibers wrapped by MBP+ oligodendrocytes. n = 2 wells per condition.
 (C) Total DAPI+ cell number for the experiment in (B).
 (D) Representative confocal images of data shown in (B). Scale bar, 100 μ m.
 (E) Inhibition of muscarinic receptor M1 by TASN-1 (100 nM) and indicated small molecules at 1 μ M, n = 2 replicated per condition.
 (F and G) Effects of tamoxifen (F), TASN-1 (100 nM), or EBP inhibitors at 1 μ M on the estrogen-dependent growth of T47D cells, n = 8 replicates per condition.
 (H) Activation of κ -opioid receptor (OPRD1) by U50488 (2 μ M), TASN-1 (100 nM), and indicated small molecules at 1 μ M, n = 2 replicates per condition.
 (I) Structures and canonical targets of molecules that can inhibit EBP.
 Data in (F and G) are represented as means \pm SD.

development potential. Hence, the leading EBP inhibitors identified in our screen as well as a previously characterized EBP inhibitor, TASN-1 (DeBrabander et al., 2016), were tested in established cell-based assays for the M1 muscarinic receptor (clemastine), the estrogen receptor (tamoxifen), and the kappa opioid receptor (U50488). While clemastine, tamoxifen, and U50488 were highly effective for their respective targets, CW9956, CW9009, CW3388, and TASN-1 showed little affinity for any of these receptors (Figures 4E–4I). Although CW9009, its analogs, and TASN-1 may have cellular targets beyond EBP, these molecules lack the highly potent off-target effects common to other EBP-inhibiting scaffolds identified in drug repurposing screens, which may be beneficial during future optimization of these scaffolds.

DISCUSSION

Here we used high-throughput screening of a structurally diverse chemical library to corroborate and significantly extend our previous finding that most enhancers of oligodendrocyte formation inhibit enzymes in cholesterol biosynthesis. Elucidation of the targets of our screening hits revealed that the majority increased oligodendrocyte formation by inhibiting CYP51, TM7SF2, or EBP. Evaluation of one series of hits revealed a broad correlation between EBP inhibition and enhanced oligodendrocyte formation. Notably, all analogs that converted the tertiary amine functionality to the derived amide lost activity in our oligodendrocyte formation assay (Figures 3B and 3D; Data S2). This finding suggests an amine is critical for inhibition of

EBP, possibly because cationic molecules can better mimic EBP's zymosterol cation intermediate. Finally, some analogs of our EBP-inhibiting leads showed affinity not for EBP but for TM7SF2 or DHCR7. Such a shift in target selectivity has been seen previously and likely reflects the similar binding pockets for these enzymes, each of which metabolize structurally similar sterols via sterol cation intermediates (Shefer et al., 1998).

SIGNIFICANCE

Here we establish that most validated enhancers of oligodendrocyte formation identified from a structurally diverse small-molecule screening library inhibit CYP51, TM7SF2, or EBP, mirroring past findings from US Food and Drug Administration-approved drugs libraries. Evaluation of analogs revealed a broad correlation between potency for EBP inhibition and oligodendrocyte formation and also identified a more potent analog that lacks the off-target effects common to past hits. These findings reinforce that modulation of the cholesterol biosynthesis pathway is a common mechanism for oligodendrocyte-enhancing small molecules and provide lead molecules for further optimization.

STAR★METHODS

Detailed methods are provided in the online version of this paper and include the following:

- **KEY RESOURCES TABLE**
- **CONTACT FOR REAGENT AND RESOURCE SHARING**
- **EXPERIMENTAL MODEL AND SUBJECT DETAILS**
 - Mouse OPC Preparation
 - Mouse OPC Culture
- **METHOD DETAILS**
 - High-Throughput Screening of 10,000 Molecules
 - In Vitro Phenotypic Screening of OPCs
 - High-Content Imaging and Analysis
 - GC/MS-Based Sterol Profiling
 - EBP Enzymatic Assay
 - Estrogen-Dependent Cell Proliferation Assay
 - Muscarinic Receptor Antagonism Assay
 - κ -opioid Receptor Agonism Assay
 - In Vitro Remyelination on Microfibers
- **QUANTIFICATION AND STATISTICAL ANALYSIS**

SUPPLEMENTAL INFORMATION

Supplemental Information includes four figures and three data files and can be found with this article online at <https://doi.org/10.1016/j.chembiol.2019.01.004>.

ACKNOWLEDGMENTS

This work was supported by NIH grant NS095280 (to P.J.T.), a Conrad N. Hilton Foundation Pilot Innovator in MS Award (to D.J.A.), a Mallinckrodt Foundation Grant Award (to D.J.A.), F30MH116581 (to Z.H.), NIH TL1 TR000441 (to Z.H.), the Peterson, Fakhouri, Long, Goodman, Geller, Judge, and Weidenthal families, CWRU School of Medicine, and the Case Comprehensive Cancer Center

(P30 CA043703). The authors thank Y. Fedorov, M. Drumm, O. Iyoha-Bello, J. Pink., P. Conrad, and ThermoFisher for technical assistance.

AUTHOR CONTRIBUTIONS

D.A. and D.J.A. evaluated the effects of small molecules on oligodendrocyte formation. D.A., Z.H., I.B., and D.J.A. performed and analyzed sterol profiling experiments. D.A. and Z.H. performed EBP biochemical assays and microfiber assays. F.J.N., H.T., W.S., and P.J.T. performed high-throughput screening. D.A., Z.H., and D.J.A. analyzed all data and wrote the manuscript. All authors provided intellectual input, edited and approved the final manuscript.

DECLARATION OF INTERESTS

The authors declare the following competing interests: D.J.A., P.J.T., F.N., Z.H., and D.A. are inventors on patents and patent applications that relate to this work and have been licensed to Convelo Therapeutics, which seeks to develop remyelinating therapeutics. D.J.A. and P.J.T. hold equity in Convelo and receive consulting income from Convelo.

Received: October 3, 2018

Revised: November 15, 2018

Accepted: January 10, 2019

Published: February 14, 2019

REFERENCES

- Bechler, M.E., Byrne, L., and Ffrench-Constant, C. (2015). CNS myelin sheath lengths are an intrinsic property of oligodendrocytes. *Curr. Biol.* 25, 2411–2416.
- DeBrabander, J., Nijhawan, D., Wang, W., Shay, J.W., and Theodoropoulos, P. (2016). Targeting emopamil binding protein with small molecules that induce an abnormal feedback response by lowering endogenous cholesterol biosynthesis. Patent WO 2017/011215, filed July 5, 2016, published January 19, 2017.
- Deshmukh, V.A., Tardif, V., Lyssiotis, C.A., Green, C.C., Kerman, B., Kim, H.J., Padmanabhan, K., Swoboda, J.G., Admad, I., Kondo, T., et al. (2013). A regenerative approach to the treatment of multiple sclerosis. *Nature* 502, 327–332.
- Fancy, S.P., Kotter, M.R., Harrington, E.P., Huang, J.K., Zhao, C., Rowitch, D.H., and Franklin, R.J. (2010). Overcoming remyelination failure in multiple sclerosis and other myelin disorders. *Exp. Neurol.* 225, 18–23.
- Franklin, R.J., and Ffrench-Constant, C. (2008). Remyelination in the CNS: from biology to therapy. *Nat. Rev. Neurosci.* 9, 839–855.
- Giera, M., Müller, C., and Bracher, F. (2015). Analysis and experimental inhibition of distal cholesterol biosynthesis. *Chromatographia* 78, 343–358.
- Gonzalez, G.A., Hofer, M.P., Syed, Y.A., Amaral, I.A., Rundle, J., Rahman, S., Zhao, C., and Kotter, M.R.N. (2016). Tamoxifen accelerates the repair of demyelinated lesions in the central nervous system. *Sci. Rep.* 6, 31599.
- Huang, J.K., Jarjour, A.A., Oumesmar, B.N., Kerinon, C., Williams, A., Krezel, W., Kagechika, H., Bauer, J., Zhao, C., Evercooren, A.B.V., et al. (2011). Retinoid X receptor gamma signaling accelerates CNS remyelination. *Nat. Neurosci.* 14, 45–53.
- Hubler, Z., Allimuthu, D., Bederman, I., Elliott, M.S., Madhavan, M., Allan, K.C., Shick, H.E., Garrison, E., Karl, M.T., Factor, D.C., et al. (2018). Accumulation of 8,9-unsaturated sterols drives oligodendrocyte formation and remyelination. *Nature* 560, 372–376.
- Keirstead, H.S., and Blakemore, W.F. (1999). The role of oligodendrocytes and oligodendrocyte progenitors in CNS remyelination. *Adv. Exp. Med. Biol.* 468, 183–197.
- Korade, Z., Kim, H.H., Tallman, K.A., Liu, W., Koczok, K., Balogh, I., Xu, L., Mirnics, K., and Porter, N.A. (2016). The effect of small molecules on sterol homeostasis: measuring 7-dehydrocholesterol in Dhcr7-deficient neuro2a cells and human fibroblasts. *J. Med. Chem.* 59, 1102–1115.
- Lariosa-Willingham, K.D., Rosler, E.S., Tung, J.S., Dugas, J.C., Collins, T.L., and Leonoudakis, D. (2016). A high throughput drug screening assay to identify

compounds that promote oligodendrocyte differentiation using acutely dissociated and purified oligodendrocyte precursor cells. *BMC Res. Notes* 9, 419.

Lassmann, H. (2001). Classification of demyelinating diseases at the interface between etiology and pathogenesis. *Curr. Opin. Neurol.* 14, 253–258.

Mei, F., Fancy, S.P.J., Shen, Y.A., Niu, J., Zhao, C., Presley, B., Miao, E., Lee, S., Mayoral, S.R., Redmond, S.A., et al. (2014). Micropillar arrays as a high-throughput screening platform for therapeutics in multiple sclerosis. *Nat. Med.* 20, 954–960.

Mei, F., Mayoral, S.R., Nobuta, H., Desponts, C., Lorrain, D.S., Xiao, L., Green, A.J., Rowitch, D., Whistler, J., and Chan, J.R. (2016). Identification of the kappa-opioid receptor as a therapeutic target for oligodendrocyte remyelination. *J. Neurosci.* 36, 7925–7935.

Moebius, F.F., Reiter, R.J., Bermoser, K., Glossmann, H., Cho, S.Y., and Paik, Y.K. (1998). Pharmacological analysis of sterol delta8-delta7 isomerase proteins with [³H]ifenprodil. *Mol. Pharmacol.* 54, 591–598.

Najm, F.J., Madhavan, M., Zaremba, A., Shick, H.E., Karl, R.T., Factor, D.C., Miller, T.E., Nevin, Z.S., Kantor, C., Sargent, A., et al. (2015). Drug-based modulation of endogenous stem cells promotes functional remyelination in vivo. *Nature* 522, 216–220.

Najm, Fadi J., Zaremba, A., Caprariello, A.V., Nayak, S., Freundt, E.C., Scacheri, P.C., Miller, R.H., and Tesar, P.J. (2011). Rapid and robust generation of functional oligodendrocyte progenitor cells from epiblast stem cells. *Nat. Methods* 8, 957–962.

Pink, J.J., and Jordan, V.C. (1996). Models of estrogen receptor regulation by estrogens and antiestrogens in breast cancer cell lines. *Cancer Res.* 56, 2321–2330.

Shefer, S., Salen, G., Honda, A., Batta, A.K., Nguyen, L.B., Tint, G.S., Ioannou, Y.A., and Desnick, R. (1998). Regulation of rat hepatic 3beta-hydroxysterol delta7-reductase: substrate specificity, competitive and non-competitive inhibition, and phosphorylation/dephosphorylation. *J. Lipid Res.* 39, 2471–2476.

STAR★METHODS

KEY RESOURCES TABLE

REAGENT or RESOURCE	SOURCE	IDENTIFIER
Antibodies		
CD140a-APC	eBioscience	Cat# 17-1401; RRID: AB529482
NG2-AF488	Millipore Sigma	Cat# AB5320A4
Anti-rat Myelin basic protein	Abcam	Cat# ab7349; RRID: AB308569
Biological Samples		
Microsomes 20mg/mL Mouse (CD1)	Thermo Fisher Scientific	Cat# MSMCPL
Chemicals, Peptides, and Recombinant Proteins		
Normal donkey serum	Jackson Immunoresearch Lab	Cat# 017-000-121
Noggin	R&D Systems	Cat#6057-NG-100
Neurotrophin 3	R&D Systems	Cat#GF031
Sonic Hedgehog	R&D Systems	Cat#8908SH-005/CF
cAMP	Millipore Sigma	Cat#A9501
IGF-1	R&D Systems	Cat#291-G1-01M
DMEM/F12	Thermo Fisher Scientific	Cat# 11320082
N2-MAX	R&D Systems	Cat# AR009
B-27	Thermo Fisher Scientific	Cat#12587010
FGF2	R&D Systems	Cat#233-FB
PDGF-AA	R&D Systems	Cat#221-AA
Laminin	Millipore Sigma	Cat# L2020
poly-ornithine	Millipore Sigma	Cat# P3655
Glutamax-1 (100x)	Gibco-Life Technologies	Cat#35050-061
poly-D-lysine	Millipore Sigma	Cat# P7886
Dimethylsulfoxide	Millipore Sigma	Cat# D8418
16% paraformaldehyde	Ted Pella Inc	Cat# 18505
Triton X-100	Millipore Sigma	Cat#T8787
25,26,26,27,27,27- ² H ₇ -cholesterol	Cambridge Isotope Lab	Cat# DLM-3057
bis(trimethylsilyl)trifluoroacetamide	Millipore Sigma	Cat# 15222-10X1ML
FF-Mas	Avanti Polar Lipids Inc	Cat# 700077
Cholesterol	Millipore Sigma	Cat# C3045-5g
Zymosterol	Avanti Polar Lipids Inc	Cat# 700118P-1mg
Desmosterol	Avanti Polar Lipids Inc	Cat# 700060
7-dehydrocholesterol	Avanti Polar Lipids Inc	Cat# 700066
Lanosterol	Avanti Polar Lipids Inc	Cat#700063-1mg
Lathosterol	Avanti Polar Lipids Inc	Cat#700069
Liothyronine (3,3,5'-Triiodo-L-thyronine)	Cayman Chemicals	Cat# 16028
Clemastine fumarate	Cayman Chemicals	Cat#14637
Ro-48-8071	Cayman Chemicals	Cat#161582-11-2
Amorolfine	Selleck Chemicals	Cat#S1676
TASIN-1	Synthesized as reported	
Zymosterol	AvantiPolar Lipids	Cat#700068P-1mg
DAPI	Millipore Sigma	Cat#D9542
Accutase	Innovative Cell Technologies	Cat#AT-104
Hoechst 33258	Sigma-Aldrich	Cat# 861405

(Continued on next page)

Continued

REAGENT or RESOURCE	SOURCE	IDENTIFIER
Critical Commercial Assays		
Muscarinic Receptor Antagonism Assay	Thermo Fisher Scientific	Select Screen cell-based GPCR profiling
κ -opioid receptor agonism assay	Thermo Fisher Scientific	Select Screen cell-based GPCR profiling
Experimental Models: Cell Lines		
EpiSC-derived OPCs	OPC-5 (XX) and OPC-1 (XY) were generated from epiblast stem cell lines generated within the Tesar Lab at CWRU.	Najm et al., 2011
T47D	Translational Research Core of the Case Comprehensive Cancer Center	
Software and Algorithms		
Operetta High Content Imaging and Analysis system	Perkin Elmer	Cat# HH12000000
PerkinElmer Harmony and Columbus software	Perkin Elmer	Cat# HH17000001
Other		
384-well, CellCarrier Ultra plates	Perkin Elmer	Cat#6057500
96-well CellCarrierUltra plates	Perkin Elmer	Cat# 6005450
Aligned fibre scaffold in insert	Amsbio	Cat# TECL006-1x

CONTACT FOR REAGENT AND RESOURCE SHARING

Further information and requests for resources and reagents should be directed to and will be fulfilled by the Lead Contact, Drew J. Adams (drew.adams@case.edu).

EXPERIMENTAL MODEL AND SUBJECT DETAILS

Mouse OPC Preparation

EpiSC-derived OPCs were previously obtained using *in vitro* differentiation protocols and culture conditions ([Najm et al., 2011](#)). Briefly, OPCs tested here were derived from two separate EpiSC lines developed from the 129SvEv mouse strain using cells isolated at E5.5, EpiSC5 (giving rise to OPC-5 OPCs and originating from a female) and 129O1 (giving rise to OPC-1 OPCs and originating from a male). To ensure uniformity throughout all *in vitro* screening experiments, EpiSC-derived OPCs were sorted to purity by fluorescence activated cell sorting at passage five with conjugated CD 140a-APC (eBioscience, 17-1401; 1:80) and NG2-AF488 (Millipore, AB5320A4; 1:100) antibodies. Sorted batches of OPCs were expanded and frozen down in aliquots. OPCs were thawed into growth conditions for one passage before use in further assays. Cultures were regularly tested and shown to be mycoplasma free and authenticated on the basis of immunopositivity for OPC markers (NG2, CD 140a) and ability to differentiate to MBP+ oligodendrocytes in the presence of thyroid hormone.

Mouse OPC Culture

EpiSC-derived OPCs were grown and expanded in poly-ornithine (PO) and laminin-coated flasks with growth medium (DMEM/F12 supplemented with N2-MAX (R&D Systems), B-27 (ThermoFisher), GlutaMax (Gibco), FGF2 (10 μ g/mL, R&D systems, 233-FB-025) and PDGF-AA (10 μ g/mL, R&D systems, 233-AA-050) before harvesting for plating.

METHOD DETAILS

High-Throughput Screening of 10,000 Molecules

At the Drug Discovery Center of the University of Cincinnati College of Medicine, EpiSC-derived OPCs were grown and expanded in poly-ornithine and laminin-coated flasks before harvesting for plating. Cells were dispensed in differentiation media supplemented with Noggin (R&D Systems; 100 ng/ml), Neurotrophin 3 (R&D Systems; 10 ng/ml), Sonic Hedgehog (R&D Systems; 200ng/ml), cAMP (Sigma; 50 μ M), and IGF-1 (R&D Systems; 100 ng/ml) using a Thermo Multidrop dispenser (ThermoFisher Scientific), into poly-D-lysine/ laminin (Sigma, L2020; 4 μ g/ml)-coated sterile, 384-well, CellCarrier Ultra plates (PerkinElmer), to a final density of 12,500 cells per well and allowed to attach for 45 min before addition of drug. A 10 mM stock of diverse 10,000 small molecules library in dimethylsulfoxide (DMSO) were prepared in Falcon polypropylene 384-well plates (Falcon). These were added to assay plates using a 50 nL solid pin tool attached to an automated workstation (Perkin Elmer), resulting in a final screening concentration of 10 μ M. After incubation at 37°C for 72 h, cells were fixed, washed and stained similar to 96-well OPC assay protocol, although all the washing steps were performed using a Biotek EL406 Microplate Washer Dispenser (Biotek) equipped with a 96-well aspiration manifold. Cells

were stained with DAPI (Sigma; 1 $\mu\text{g}/\text{ml}$) and MBP antibody (Abcam, ab7349; 1:100). Plates were imaged on the Opera High Content Imaging and Analysis system (PerkinElmer) and a set of 18 fields captured from each well resulting in an average of >1,000 cells being scored per well. Analysis was performed as in High-Content Imaging and Analysis, above. Plates for the primary screen were processed and analyzed in three separate runs. Molecules causing more than 20% reduction in nuclear count relative to DMSO control wells were removed from consideration, and hits were called on the basis of 1) >2-fold-increase in percentage of MBP+ oligodendrocytes relative to DMSO controls within the same plate, and 2) visual inspection to ensure that putative hit wells contained the expected increased number of cells of typical oligodendrocyte morphology.

In Vitro Phenotypic Screening of OPCs

Further analysis of HTS hits was performed at CWRU. EpiSC-derived OPCs were seeded onto poly-D-lysine 96-well CellCarrier or CellCarrierUltra plates (PerkinElmer) coated with laminin (Sigma, L2020; 15 $\mu\text{g}/\text{ml}$) using multi-channel pipet. For the experiment, 800,000 cells/mL stock in differentiation medium (DMEM/F12 supplemented with N2-MAX and B-27) was prepared and stored on ice for 2 h. Then, 40,000 cells were seeded per well in differentiation medium and allowed to attach for 30 min before addition of drug. For dose-response testing of all molecules, a 1000x compound stock in dimethyl sulphoxide (DMSO) was added to assay plates with 0.1 μL solid pin multi-blot replicators (V & P Scientific; VP 409), resulting in a final screening concentration of 1x. Cells were incubated under standard conditions (37°C, 5% CO₂) for 3 days and fixed with 4% paraformaldehyde (PFA) in phosphate buffered saline (PBS) for 20 min. Fixed plates were washed with PBS (200 μL per well) twice, permeabilized with 0.1% Triton X-100 and blocked with 10% donkey serum (v/v) in PBS for 40 min. Then, cells were labelled with an anti-MBP antibody (Abcam, ab7349; 1:200) for 16 h at 4°C followed by detection with Alexa Fluor conjugated secondary antibodies (1:500) for 45 min. Nuclei were visualized by DAPI staining (Sigma; 1 $\mu\text{g}/\text{ml}$). During washing steps, PBS was added using a multi-channel pipet and aspiration was performed using Biotek EL406 washer dispenser (Biotek) equipped with a 96-well aspiration manifold.

High-Content Imaging and Analysis

During hit validation experiments, plates were imaged on the Operetta High Content Imaging and Analysis system (PerkinElmer) and a set of 6 fields captured from each well resulting in an average of 1,200 cells being scored per well. Analysis (PerkinElmer Harmony and Columbus software) began by identifying intact nuclei stained by DAPI; that is, those traced nuclei that were larger than 300 μm^2 in surface area. Each traced nucleus region was then expanded by 50% and cross-referenced with the mature myelin protein (MBP) stain to identify oligodendrocyte nuclei, and from this the percentage of oligodendrocytes was calculated.

GC/MS-Based Sterol Profiling

EpiSC-derived OPCs were plated at 0.5 million cells per ml in PDL- and laminin-coated six or twelve well plate with differentiation media. After 24 hours, cells were dissociated with Accutase, rinsed with saline, and cell pellets were frozen. For sterol analyses, cells were lysed in methanol (Sigma-Aldrich) with agitation for 30 minutes and cell debris removed by centrifugation at 10,000 rpm for 15 min. Cholesterol-d7 standard (25,26,26,26,27,27,27,27-²H₇-cholesterol, Cambridge Isotope Laboratories) was added before drying under nitrogen stream and derivatization with 55 μL of bis(trimethylsilyl)trifluoroacetamide/trimethylchlorosilane to form trimethylsilyl derivatives. Following derivatization at 60°C for 20 minutes, 1 μL was analyzed by gas chromatography/mass spectrometry using an Agilent 5973 Network Mass Selective Detector equipped with a 6890 gas chromatograph system and a HP-5MS capillary column (60 m x 0.25 mm x 0.25 μm). Samples were injected in splitless mode and analyzed using electron impact ionization. Ion fragment peaks were integrated to calculate sterol abundance, and quantitation was relative to cholesterol-d7. The following m/z ion fragments were used to quantitate each metabolite: cholesterol-d7 (465), FF-Mas (482), cholesterol (368), zymostenol (458), zymosterol (456), desmosterol (456, 343), 7-dehydrocholesterol (456, 325), lanosterol (393), lathosterol (458), 14-dehydrozymostenol (456). Calibration curves were generated by injecting varying concentrations of sterol standards and maintaining a fixed amount of cholesterol-D7.

EBP Enzymatic Assay

EBP enzymatic activity was measured using a reported method with slight modifications (Moebius et al., 1998): active EBP was obtained from mouse microsomes, inhibitors were added, zymostenol was added at a final concentration of 25 μM in a final reaction volume of 500 μL , and the reaction incubated at 37°C for 2 h. Sterols were extracted using 3 x 1 ml hexanes, cholesterol-d7 was added to enable quantitation, and the pooled organics were dried (Na₂SO₄) and evaporated under nitrogen gas. Samples were then silylated and analyzed using GC/MS as described above.

Estrogen-Dependent Cell Proliferation Assay

Estrogen-dependent cell proliferation was measured as previously described with minor modifications (Pink and Jordan, 1996). After growth in estrogen-free media (Phenol red-free RPMI supplemented with 10% charcoal stripped fetal bovine serum) for 5 days, cells were seeded at 2,500 cells/well into 96 well plates. The following day 3x drug containing media was added to triplicate wells and cells were allowed to grow for an additional 5 days at 37°C in standard a 5% CO₂ humidified incubator. Total DNA per well was measured. At this time media was removed, cells were washed one time with 0.25x PBS and 100 μL of distilled water was added. Plates were frozen and thawed to enhance cell lysis and 200 μL of 10 $\mu\text{g}/\text{ml}$ Hoechst 33258 (Sigma-Aldrich, St. Louis, MO.) in 2 M NaCl, 1 mM EDTA, 10 mM Tris-HCl pH 7.4 was added. After incubation at room temperature for 2 hours, plates were read in a SpectraMax i3

fluorescent plate reader (Molecular Devices, Sunnyvale, CA) with excitation at 360nm and emission at 460 nm. All values were converted to microgram DNA per well using a standard curve derived from purified salmon testes DNA.

Muscarinic Receptor Antagonism Assay

GeneBLAzer M1-NFAT-*bla* CHO-K1 cells (ThermoFisher) were thawed into Assay Media (DMEM, 10% dialyzed FBS, 25 mM HEPES pH 7.3, 0.1 mM NEAA). 10,000 cells/well were added to a 384-well TC treated assay plate and incubated 16-24 h at 37°C. 4 μ l of a 10x stock of antimuscarinic molecules was added to the plate and incubated 30 min. 4 μ l of 10x control agonist Carbachol at the pre-determined EC80 concentration was added to wells containing antimuscarinic molecules. The plate was incubated 5 h and 8 μ l of 1 μ M Substrate + Solution D Loading Solution was added to each well and the plate was incubated 2 h at room temperature before reading on a fluorescence plate reader.

κ -opioid Receptor Agonism Assay

Tango-*bla* U2OS cells OPRD1 (ThermoFisher) were thawed into Assay Media (DMEM, 10% dialysed FBS, 25 mM HEPES pH 7.3, 0.1 mM NEAA). 10,000 cells/well were added to a 384-well TC treated assay plate. 8 μ l of a 5x stock of test molecules or agonist (U50488) were added to the plate and incubated 16 h at 37°C. The plate was added with 8 μ l of 1 μ M substrate + solution D loading solution was added to each well and the plate was incubated 2 h in dark at room temperature before reading on a fluorescence plate reader. The DMSO treatment condition was normalized to 0% and the positive control treatment was normalized to 100%. This cell line was validated in each run on the basis of $z' > 0.5$ for agonist U50488 versus control treatment.

In Vitro Remyelination on Microfibers

A 12-well plate containing Mimetex aligned scaffold (microfiber plate, AMSBIO, AMS.TECL-006-1X, Electrospun poly-L-lactide Scaffold, 2 μ M fibre diameter cell crown inserts) was prepared as previously described (Hubler et al., 2018). Briefly, fiber inserts were sterilized with 70% ethanol and washed with PBS before being coated with polyornithine and laminin. After laminin coating, 100,000 cells/mL of EpiSC-derived OPCs (1.5 mL/well) were plated in differentiation medium. After 24 h the media was replaced with fresh media containing small molecule treatments. Every 48 h the media was replaced with fresh compound containing media for the first 4 days of 14 days culture. Microfibre inserts were fixed with 4% PFA, permeabilized with 0.1% Triton X-100, and blocked with 10% donkey serum (v/v) in PBS for 60 min. Then stained for MBP (Abcam, ab7349; 1:100) and DAPI staining (Sigma; 5 μ g/ml). After staining, the fiber inserts were mounted on a glass slide (Fisherbrand Superfrost Plus Microscope Slides) using Fluormount-G (Southern Biotech) with a cover glass (Fisherbrand Microscope Cover Glass) and dried at RT in dark for 36 h. The mounted inserts were imaged on the Operetta High Content Imaging and Analysis system (PerkinElmer) and a set of 22 fields captured from each condition resulting in an average of 2000 cells being scored per well. The total microfiber area was calculated using bright field imaging and a spot-finding function (area larger than 2 μm^2). The MBP+ pixel area within the defined microfiber area was then defined and the percentage of the total microfiber area calculated. In addition, confocal imaging was performed with Operetta high-content imaging system to visualize the wrapping of myelin around the microfibers.

QUANTIFICATION AND STATISTICAL ANALYSIS

No statistical methods were used to predetermine sample size. Number of replicates and independent experiments performed are noted in the figure legend. Data were expressed as mean \pm s.d. and *P* values in Figure 2H were calculated using an unpaired two-tailed Student's *t*-test for pairwise comparison of variables with a 95% confidence interval and $n - 2$ degrees of freedom, where *n* is the total number of samples.